STUDY OF CP VIOLATION IN B MESONS USING THE *BABAR* DETECTOR

David J. Lange[*]

Lawrence Livermore National Laboratory

Mail Stop L-050, 7000 East Ave, Livermore, Ca 94550

Representing the *BABAR* Collaboration

ABSTRACT

We present results on time-dependent CP asymmetries in neutral B decays. The measurements use a data sample of about 88 million $\Upsilon(4S) \rightarrow B\bar{B}$ decays collected between 1999 and 2002 with the *BABAR* detector at the PEP-II asymmetric-energy B Factory at SLAC. We study events in which one neutral B meson is fully reconstructed in a final state and the other B meson is determined to be either a B^0 or $\bar{B}^0$ from its decay products. Final states considered include $B^0 \rightarrow J/\psi\, K^0_S$, $B^0 \rightarrow J/\psi\, K^0_L$, $B^0 \rightarrow J/\psi\, \pi^0$, $B^0 \rightarrow D^{*+}D^{*-}$, $B^0 \rightarrow \phi K^0_S$, $B^0 \rightarrow \pi^+\pi^-$, and $B^0 \rightarrow \rho^{\pm}\pi^{\mp}$.

---

1 Introduction

Measurements[1–6] of time dependent decay rates in $\Upsilon(4S) \to B^0\overline{B}^0$ decays have been performed using the *BABAR*[7] detector. CP violating asymmetries arise from the interference of multiple decay amplitudes and have a variety of possible experimental signatures. In the case described here, the decay rates for B^0 and $\overline{B}^0$ (at $t=0$) mesons to a common final state f have a different time dependence

$$\frac{d\Gamma(B^0 \to f)}{dt} \neq \frac{d\Gamma(\overline{B}^0 \to f)}{dt}.$$ (1)

In $\Upsilon(4S) \to B^0\overline{B}^0$ decays, the magnitude of the interfering amplitudes are comparable, which lead to possibly large asymmetries in the Standard Model. While the branching fractions for common final states are small ($\leq 10^{-3}$), sizable samples of these states have been reconstructed in approximately 88×10^6 $B\bar{B}$ decays collected in between October 1999 and 2002 by the *BABAR* experiment.

CP-violation is accommodated in the Standard Model through a complex phase within the CKM matrix[8]

$$V_{CKM} \equiv \begin{pmatrix} V_{ud} & V_{us} & V_{ub} \\ V_{cd} & V_{cs} & V_{cb} \\ V_{td} & V_{ts} & V_{tb} \end{pmatrix},$$ (2)

that describes the coupling for charged weak transitions $q \to W^{*+}q'$ ($\propto V_{qq'}^*$). The orthogonality of the first and third columns

$$V_{ud}V_{ub}^* + V_{cd}V_{cb}^* + V_{td}V_{tb}^* = 0$$ (3)

gives the "Unitarity Triangle" shown in Figure 1, and defines the angles α, β, and γ. Together with other measurements[9] (such as ϵ_k , $|V_{ub}|$, $|V_{cb}|$, Δm_d, and Δm_s), measurements of CP violating asymmetries over-constrain the Unitarity Triangle, and thus are a test of the Standard Model. Unlike other constraints, the measurement of $\sin 2\beta$ using $b \to c\bar{c}s$ charmonium-containing modes discussed here is essentially free of theoretical uncertainties.

$B^0\overline{B}^0$ pairs are produced in a coherent $L=1$ state at the $\Upsilon(4S)$. Thus, the decay distribution for $B \to f$, where f is a CP eigenstate, depends on Δt, the difference between the decay time of the B that decays to f (B_{CP}) and the other B in the event (B_{tag}).
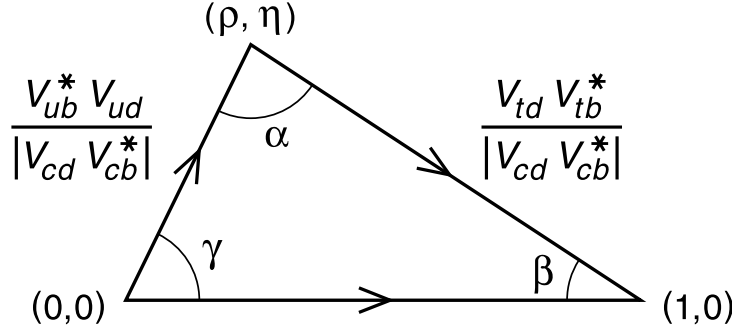
Fig. 1. The normalized Unitarity Triangle determined from the orthogonality of the first and third columns of the CKM matrix.

The proper-time distribution of B meson decays to a CP eigenstate with a B^0 or $\overline{B}^0$ tag can be expressed in terms of a complex parameter λ that depends on both the B^0-$\overline{B}^0$ oscillation amplitude and the amplitudes describing $\overline{B}^0$ and B^0 decays to this final state.[10] The decay rate $\mathrm{f}_+(\mathrm{f}_-)$ when the tagging meson is a $B^0(\overline{B}^0)$ is given by

$$\mathrm{f}_\pm(\Delta t) = \frac{e^{-|\Delta t|/\tau_{B^0}}}{4\tau_{B^0}} \left[1 \pm S_f \sin\left(\Delta m_d \Delta t\right) \mp C_f \cos\left(\Delta m_d \Delta t\right) \right], \qquad (4)$$

where

$$\begin{aligned} S_f &= \frac{2\,\mathcal{I}m\,\lambda}{1+|\lambda|^2}, \\ C_f &= \frac{1-|\lambda|^2}{1+|\lambda|^2}, \end{aligned} \qquad (5)$$

$\Delta t = t_{\mathrm{rec}} - t_{\mathrm{tag}}$ is the difference between the proper decay times of the reconstructed B meson (B_{CP}) and the tagging B meson (B_{tag}), τ_{B^0} is the B^0 lifetime, and Δm_d is the B^0-$\overline{B}^0$ oscillation frequency. The sine term in Eq. 4 is due to the interference between direct decay and decay after flavor change, and the cosine term is due to the interference between two or more decay amplitudes with different weak and strong phases. CP violation can be observed as a difference between the Δt distributions of B^0- and $\overline{B}^0$-tagged events or as an asymmetry with respect to $\Delta t = 0$ for either flavor tag.

The Δt asymmetry is

$$A_{CP}(\Delta t) \equiv \frac{\mathrm{f}_+(\Delta t) - \mathrm{f}_-(\Delta t)}{\mathrm{f}_+(\Delta t) + \mathrm{f}_-(\Delta t)} = S_f \sin\left(\Delta m_d \Delta t\right) - C_f \cos\left(\Delta m_d \Delta t\right). \qquad (6)$$

The time integrated asymmetry is non-zero if $C_f \neq 0$.

2 Common analysis features

2.1 The *BABAR* detector

A detailed description of the *BABAR* detector can be found in elsewhere.[7] Charged particle momenta are measured in a tracking system consisting of a 5-layer double-sided silicon vertex tracker (SVT) and a 40-layer drift chamber (DCH) filled with a gas mixture based on helium and isobutane. The SVT and DCH operate within a 1.5-T superconducting solenoidal magnet. The typical decay vertex resolution is around 65 μm along the beam direction for fully reconstructed B decays. Photons are detected in an electromagnetic calorimeter (EMC) consisting of 6580 CsI(Tl) crystals arranged in barrel and forward end-cap sub-detectors. The π^0 mass resolution is on average 7 MeV/c^2. The flux return (IFR) for the solenoid is composed of multiple layers of iron and resistive plate chambers for the identification of muons and long-lived neutral hadrons. Tracks are identified as pions or kaons by the Cherenkov angle θ_{Ch} measured with a detector of internally reflected Cherenkov light (DIRC). The typical separation between pions and kaons varies from 8σ at 2 GeV/c to 2.5σ at 4 GeV/c, where σ is the average θ_{Ch} resolution. Lower momentum kaons are identified with a combination of θ_{Ch} (for momenta down to 0.7 GeV/c) and measurements of ionization energy loss, dE/dx, in the DCH and SVT.

2.2 Data sample

The analysis described here use a data sample of approximately 88 million $B^0\overline{B}^0$ decays, corresponding to 81 fb^{-1}. An additional 9.6 fb^{-1} taken around 40 MeV below the $\Upsilon(4S)$ resonace ("off-resonance" sample) is used to study $e^+e^- \to q\bar{q}$ ("continuum") backgrounds that are important in several of the analysis described here.

2.3 Analysis procedure

The decay channels described in this note share many common analysis features. In each case, one of the two B decays B_{CP} is fully reconstructed, while the other B_{tag} is inclusively reconstructed to determine ("tag") the flavor of B_{CP} at $\Delta t = 0$. Due primarily to limitations of the B_{tag} reconstruction, Eq. 4 must be modified for experimental effects.

In particular, a flavor mistag probability and vertex position resolution are accounted for

$$f_{\pm}(\Delta t) = \frac{e^{-|\Delta t|/\tau_{B^0}}}{4\tau_{B^0}} \left[1 \quad \pm \quad S_f(1 - 2w)\sin(\Delta m_d \Delta t) \right.$$
$$\left. \mp \quad C_f(1 - 2w)\cos(\Delta m_d \Delta t) \right] \otimes \mathcal{R}, \qquad (7)$$

where w is the mistag probability and $\mathcal{R}$ is the vertex resolution function. As described in the following sections, to fully exploit the available information in each event, these parameters are determined event-by-event.

As both w and $\mathcal{R}$ are dominated by properties of the B_{tag}, they are common to the B_{CP} channels described here. Instead of relying on a Monte Carlo simulation, we use a large flavor eigenstate sample B_{flav} to determine these parameters from the data. As with the B_{CP} samples, the other B decay is inclusively reconstructed to determine the Δt and flavor tag of the event. The expected Δt distribution of these events is

$$f_{\text{unmixed, mixed}}(\Delta t) = \frac{e^{-|\Delta t|/\tau_{B^0}}}{4\tau_{B^0}} \left[1 \pm (1 - 2w)\cos(\Delta m_d \Delta t) \right] \otimes \mathcal{R}, \qquad (8)$$

for unmixed ($B^0\,\overline{B}^0$) and mixed ($B^0\,B^0$ or $\overline{B}^0\,\overline{B}^0$) events.

2.4 The B_{flav} sample

The B_{flav} sample is approximately 10 times the size of the largest B_{CP} sample and consists of reconstructed $B \to D^{(*)}\pi$ $B \to D^{(*)}\rho$, $B \to D^{(*)}a_1$, and $B \to J/\psi K^*(K^\pm \pi^\mp)$ final states. Aside from D, D^*, and J/ψ mass requirements, signal events are separated from background using energy and momentum constraints on the reconstructed B_{flav} candidate. Working at the $\Upsilon(4S)$, the substitution of the measured energy by the beam energy reduces the resolution of these kinematic variables substantially.

Energy conservation can be expressed as:

$$\Delta E = E_B^* - E_{\text{beam}}^*, \qquad (9)$$

where E_B^* is the single beam energy in center-of-mass reference frame. $(E_B^*, \vec{p}^{\,*}_B)$ is the four momentum of the candidate B meson measured in the center-of-mass frame. ΔE is near 0 for correctly reconstructed B candidates, with a resolution which depends on the reconstructed channel and is typically $15 - 50$ MeV.
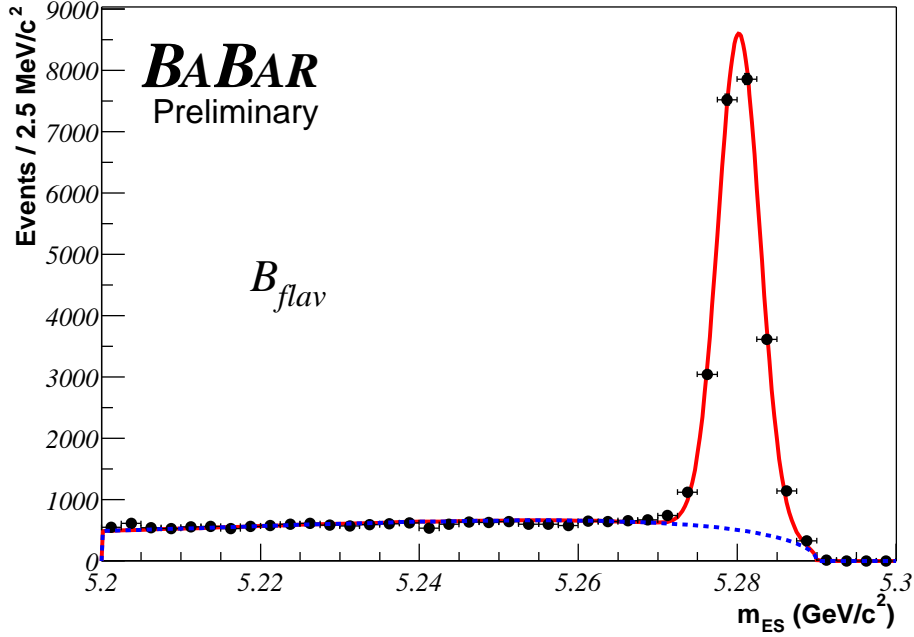
Fig. 2. m_{ES} distributions for the B_{flav} sample after all selection criteria are applied. In addition a good vertex and flavor tag are required. We observe approximately 25400 events in the signal region with a 85% purity.

Momentum conservation is expressed as the beam-energy substituted mass m_{ES}, which is defined as:

$$m_{ES} = \sqrt{E_{\mathrm{beam}}^{*2} - \vec{p}_B^{*2}}. \tag{10}$$

where $\vec{p}_B^{*}$ is the B-candidate momentum evaluated in the center-of-mass frame. Signal events are distributed Gaussian like in m_{ES} with a mean at the B mass and a resolution of approximately 2.6 MeV/c^2, dominated by the beam energy spread. The background shape in m_{ES} is parametrized by a threshold function[16] with a fixed endpoint given by the average beam energy. We typically require that $m_{ES} > 5.2\,\mathrm{GeV}/c^2$ for a B candidate to enter the analysis.

The m_{ES} distribution of the B_{flav} sample is shown in Figure 2. Figure 3 shows the Δt distribution and raw asymmetry of B^0 vs. $\overline{B}^0$ tagged events $(N_{B^0} - N_{\overline{B}^0})/(N_{B^0} + N_{\overline{B}^0})$ vs. Δt. As expected for flavor eigenstates, no asymmetry is observed.
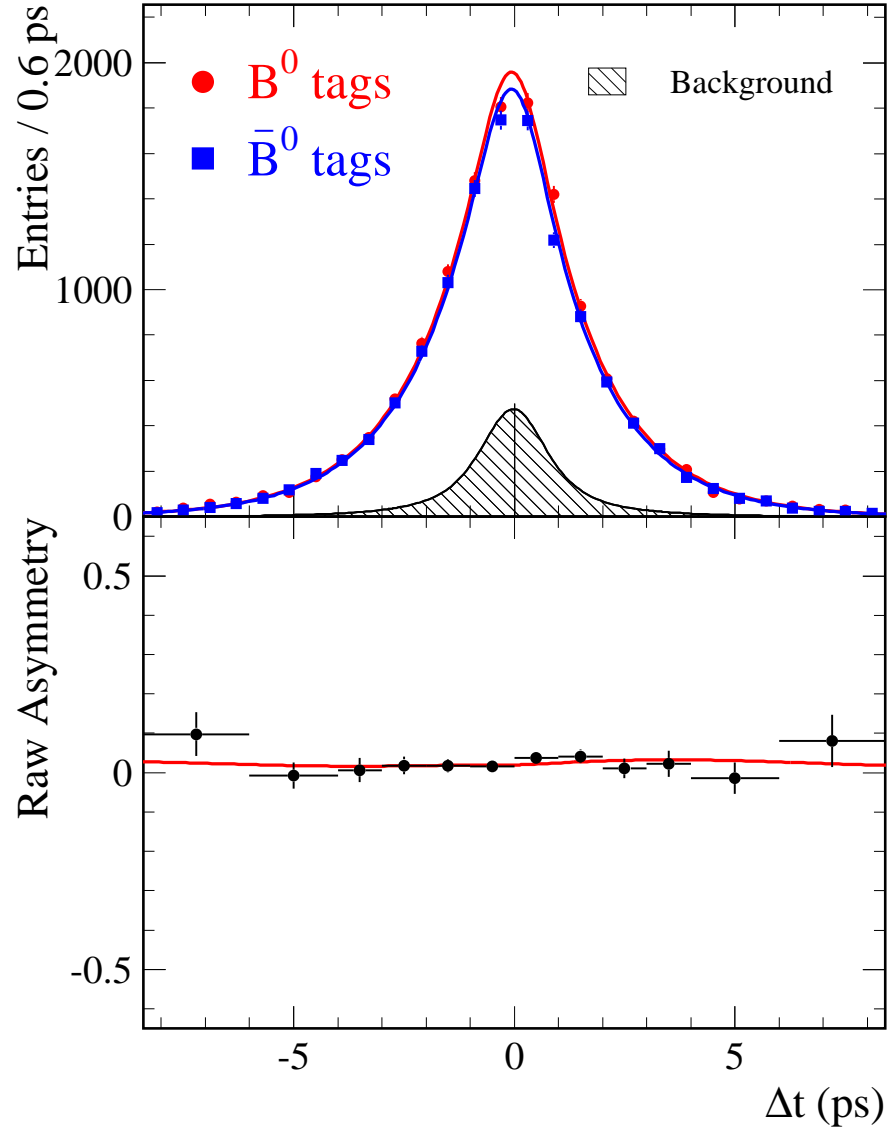
Fig. 3. Distribution of Δt for B^0 and $\overline{B}^0$ tagged events (top) and the Δt asymmetry (bottom) ($(N_{B^0} - N_{\overline{B}^0})/(N_{B^0} + N_{\overline{B}^0})$) for the B_{flav} sample.

Category	ε (%)	w (%)	Δw (%)	Q (%)
Lepton	9.1 ± 0.2	3.3 ± 0.6	-1.5 ± 1.1	7.9 ± 0.3
Kaon I	16.7 ± 0.2	10.0 ± 0.7	-1.3 ± 1.1	10.7 ± 0.4
Kaon II	19.8 ± 0.3	20.9 ± 0.8	-4.4 ± 1.2	6.7 ± 0.4
Inclusive	20.0 ± 0.3	31.5 ± 0.9	-2.4 ± 1.3	2.7 ± 0.3
All	65.6 ± 0.5			28.1 ± 0.7

Table 1. Efficiencies ϵ_i, average mistag fractions w_i, mistag fraction differences $\Delta w_i = w_i(B^0) - w_i(\overline{B}^0)$, and Q extracted for each tagging category i from the B_{flav} and B_{CP} samples.

2.5 B flavor tagging

We use multivariate algorithms to identify signatures of B decays that determine the flavor of B_{tag}. Primary leptons from semileptonic B decays are selected from identified electrons and muons as well as isolated energetic tracks. We use the charges of identified kaon candidates to define a kaon tag. Soft pions from D^{*+} decays are selected on the basis of their momentum and direction with respect to the thrust axis of B_{tag}. A neural network, which combines the outputs of these physics-based algorithms, takes into account correlations between different sources of flavor information and provides an estimate of the mistag probability for each event.

By using the outputs of the process-based algorithms and the estimated mistag probability, each event is assigned to one of four hierarchical, mutually exclusive tagging categories. The Lepton category contains events with an identified lepton, and a supporting kaon tag if present. Events with a kaon candidate and soft pion with opposite charge and similar flight direction are assigned to the Kaon I category. Events with only a kaon tag are assigned to the Kaon I or Kaon II category depending on the estimated mistag probability. The Kaon II category also contains the remaining events with a soft pion. All other events are assigned to the Inclusive category or excluded from further analysis based on the estimated mistag probability. The tagging efficiencies ε_i for the four tagging categories are measured from data and summarized in Table 1. The figure of merit for tagging is the effective tagging efficiency $Q \equiv \sum_i \varepsilon_i (1 - 2w_i)^2$. This algorithm improves Q by about 7% (relative) over our previous algorithm.[14]

2.6 Vertex reconstruction

The decay time difference Δt is determined from the distance between the decay points of B_{CP} and B_{tag}. As B mesons are produced nearly at rest in the $\Upsilon(4S)$ rest frame, the $\Upsilon(4S)$ must be produced with a boost (conventionally along the z axis) so that $\Delta z \equiv z_{CP} - z_{\text{tag}} \approx \beta\gamma c \Delta t$ can be measured. z_{CP} is the vertex position of B_{CP}. z_{tag} is determined from an iterative algorithm using the remaining tracks in the event after the B_{CP} has been reconstructed. Constraints from the beam spot location and the B_{rec} momentum are used, and large contributors to the vertex χ^2 are dropped to reduce the bias from charm decay. The determination of z_{tag} dominates the resolution of Δz. The fraction of events with a B_{CP} candidate where Δz can be determined is approximately 95%. We parametrize the experimental resolution function as the sum of three Gaussians. Two of these are a function of the determined event-by-event error and the third is an outlier contribution of fixed width (8 ps). In the unbinned maximum likelihood fit described below, the core Gaussian is determined to contain 89% of the events with a scale factor of 1.10 ± 0.05 with respect to the event-by-event error.

3 Measurement of $\sin 2\beta$ in $B \to (c\bar{c})K_S$ and $B \to J/\psi K_L^0$ decays

In the Standard Model, $\lambda = \eta_f e^{-2i\beta}$ for charmonium-containing $b \to c\bar{c}s$ decays, where η_f is the CP eigenvalue of the final state f. Thus, $S_f = -\eta_f \sin 2\beta$ and $C_f = 0$, and the time-dependent CP asymmetry is

$$A_{CP}(\Delta t) \equiv \frac{f_+(\Delta t) - f_-(\Delta t)}{f_+(\Delta t) + f_-(\Delta t)} = -\eta_f \sin 2\beta \sin (\Delta m_d \, \Delta t), \qquad (11)$$

with $\eta_f = -1$ for $J/\psi\, K_S^0$, $\psi(2S)K_S^0$, $\chi_{c1}K_S^0$, and $\eta_c K_S^0$, and $+1$ for $J/\psi\, K_L^0$. Due to the presence of even (L=0, 2) and odd (L=1) orbital angular momenta in the $B \to J/\psi\, K^{*0}$ final state, there can be CP-even and CP-odd contributions to the decay rate. When the angular information in the decay is ignored, the measured CP asymmetry in $J/\psi\, K^{*0}$ is reduced by a factor $1 - 2R_\perp$, where $R_\perp$ is the fraction of the L=1 component. We have measured $R_\perp = (16.0 \pm 3.5)\%$,[11] which gives $\eta_f = 0.65 \pm 0.07$ after acceptance corrections in the $J/\psi\, K^{*0}$ mode.

Observations of CP violation in B^0 decays were reported last year by the *BABAR*[12] and Belle[13] collaborations. The PEP-II collider has since delivered an additional 63

fb^{-1}, thereby approximately tripling the data sample near the $\Upsilon(4S)$ resonance. Here, we report a more precise measurement of $\sin2\beta$ using the full sample of about 88 million $B\bar{B}$ decays.

The measurement technique is described in detail elsewhere.[14] We reconstruct a sample of neutral B mesons (B_{CP}) decaying to the final states $J/\psi K_S^0$, $\psi(2S)K_S^0$, $\chi_{c1}K_S^0$, $\eta_c K_S^0$, $J/\psi K^{*0}(K^{*0} \to K_S^0\pi^0)$, and $J/\psi K_L^0$. The J/ψ and $\psi(2S)$ mesons are reconstructed through their decays to e^+e^- and $\mu^+\mu^-$; the $\psi(2S)$ is also reconstructed through its decay to $J/\psi\pi^+\pi^-$. We reconstruct χ_{c1} mesons in the decay mode $J/\psi\gamma$ and η_c mesons in the $K_S^0 K^+\pi^-$ and $K^+K^-\pi^0$ final states.[15] The K_S^0 is reconstructed in its decay to $\pi^+\pi^-$ (and to $\pi^0\pi^0$ for the $J/\psi K_S^0$ mode).

Figure 4 shows the m_{ES} distribution (all modes except for $B^0 \to J/\psi K_L^0$) and ΔE distribution (for $B^0 \to J/\psi K_L^0$) for events that satisfy the tagging and vertexing requirements. In total, there are 2641 in the signal region. The purity for the all modes except for $B^0 \to J/\psi K_L^0$ is very high. $B^0 \to J/\psi K_L^0$ is different from the other modes considered, as the K_L^0 energy is not fully measured by the detector (K_L^0 are reconstructed in either the EMC or IFR). Thus, one of the two degrees of freedom described above must be used to determine the K_L^0 energy. Sample purities are given in Table 2.

We determine $\sin2\beta$ with a simultaneous unbinned maximum likelihood fit to the Δt distributions of the tagged B_{CP} and B_{flav} samples. There are 34 free parameters in the fit: $\sin2\beta$ (1), the average mistag fractions w and the differences Δw between B^0 and $\bar{B}^0$ mistag fractions for each tagging category (8), parameters for the signal Δt resolution (8), and parameters for background time dependence (6), Δt resolution (3), and mistag fractions (8). We fix $\tau_{B^0} = 1.542\,\mathrm{ps}$ and $\Delta m_d = 0.489\,\mathrm{ps}^{-1}$.[17] See Fig. 5.

The fit to the B_{CP} and B_{flav} samples yields

$$\sin2\beta = 0.741 \pm 0.067\ (\mathrm{stat}) \pm 0.034\ (\mathrm{syst}).$$

The dominant sources of systematic error are the uncertainties in the level, composition, and CP asymmetry of the background in the selected CP events (0.023), the assumed parameterization of the Δt resolution function (0.017), due in part to residual uncertainties in the internal alignment of the vertex detector, and possible differences between the B_{flav} and B_{CP} mistag fractions (0.012). Most systematic errors are determined with data and will continue to decrease with additional statistics.

The large B_{CP} sample allows a number of consistency checks, including separation of the data by decay mode, tagging category, and B_{tag} flavor. The results of fits to these $\eta_f = -1$ subsamples are shown in Table 2 and found to be statistically consistent. The
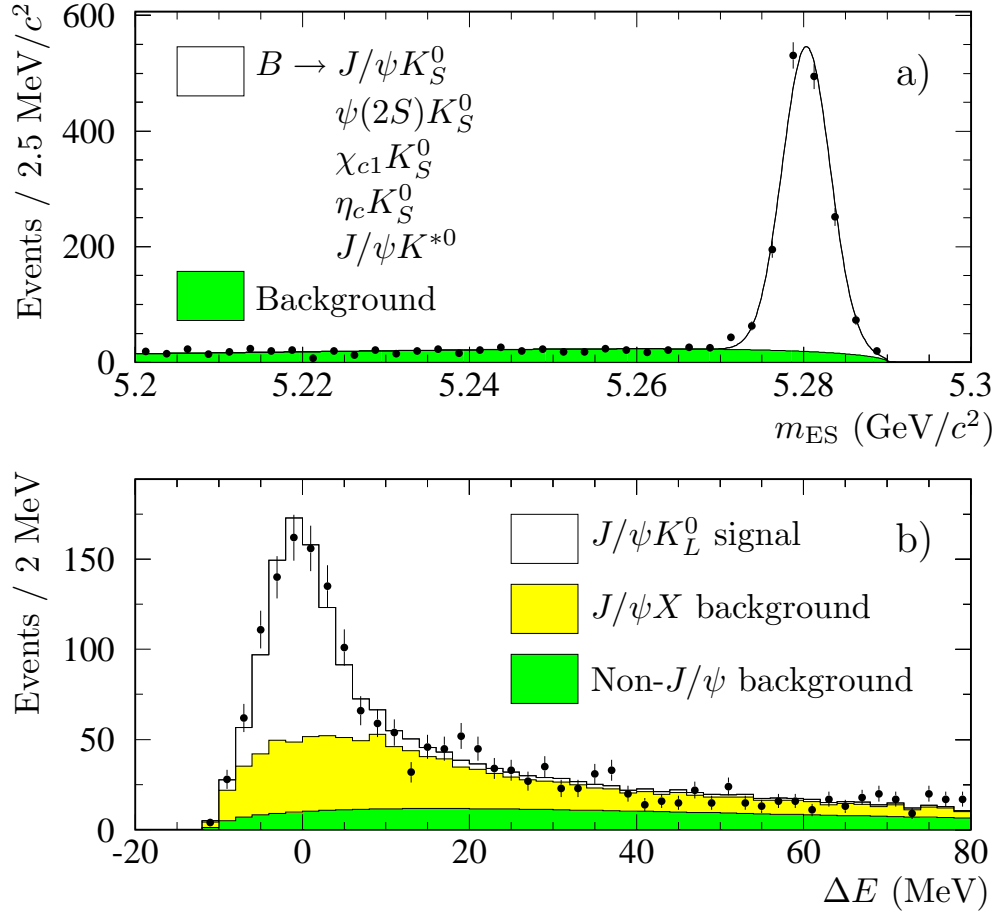
Fig. 4. Distributions for B_{CP} candidates satisfying the tagging and vertexing requirements: a) m_{ES} for the final states $J/\psi K_s^0, \psi(2S)K_s^0, \chi_{c1}K_s^0, \eta_c K_s^0$, and $J/\psi K^{*0}(K^{*0} \rightarrow K_s^0\pi^0)$, and b) ΔE for the final state $J/\psi K_L^0$.

results of fits to the control samples of non-CP decay modes indicate no statistically significant asymmetry.

Finally, we also measure the parameter $|\lambda|$ in Eq. 4 from a fit to the $\eta_f = -1$ sample, which has high purity and requires minimal assumptions on the effect of backgrounds. This parameter is sensitive to the difference in the number of B^0- and $\bar{B}^0$-tagged events. In order to account for differences in reconstruction and tagging efficiencies for B^0 and $\bar{B}^0$ mesons, we incorporate five additional free parameters in this fit. We obtain $|\lambda| = 0.948 \pm 0.051$ (stat) ± 0.030 (syst). The coefficient of the $\sin(\Delta m_d \Delta t)$ term in Eq. 4 is measured to be 0.759 ± 0.074 (stat). The dominant contribution to the systematic error for $|\lambda|$, conservatively estimated to be 0.025, is due to interference

Sample	N_{tag}	$P(\%)$	$\sin2\beta$
$J/\psi\,K_S^0, \psi(2S)K_S^0, \chi_{c1}K_S^0, \eta_c K_S^0$	1506	94	0.76 ± 0.07
$J/\psi\,K_L^0$ $(\eta_f = +1)$	988	55	0.72 ± 0.16
$J/\psi\,K^{*0}(K^{*0} \to K_S^0\pi^0)$	147	81	0.22 ± 0.52
Full CP sample	2641	78	0.74 ± 0.07
$J/\psi\,K_S^0, \psi(2S)K_S^0, \chi_{c1}K_S^0, \eta_c K_S^0$ only $(\eta_f = -1)$			
$\quad J/\psi\,K_S^0$ $(K_S^0 \to \pi^+\pi^-)$	974	97	0.82 ± 0.08
$\quad J/\psi\,K_S^0$ $(K_S^0 \to \pi^0\pi^0)$	170	89	0.39 ± 0.24
$\quad \psi(2S)K_S^0$ $(K_S^0 \to \pi^+\pi^-)$	150	97	0.69 ± 0.24
$\quad \chi_{c1}K_S^0$	80	95	1.01 ± 0.40
$\quad \eta_c K_S^0$	132	73	0.59 ± 0.32
`Lepton` category	220	98	0.79 ± 0.11
`Kaon I` category	400	93	0.78 ± 0.12
`Kaon II` category	444	93	0.73 ± 0.17
`Inclusive` category	442	92	0.45 ± 0.28
B^0 tags	740	94	0.76 ± 0.10
$\overline{B}^0$ tags	766	93	0.75 ± 0.10
B_{flav} sample	25375	85	0.02 ± 0.02
B^+ sample	22160	89	0.02 ± 0.02

Table 2. Number of events N_{tag} in the signal region after tagging and vertexing requirements, signal purity P, and results of fitting for CP asymmetries in the B_{CP} sample and in various subsamples, as well as in the B_{flav} and charged B control samples. Errors are statistical only.
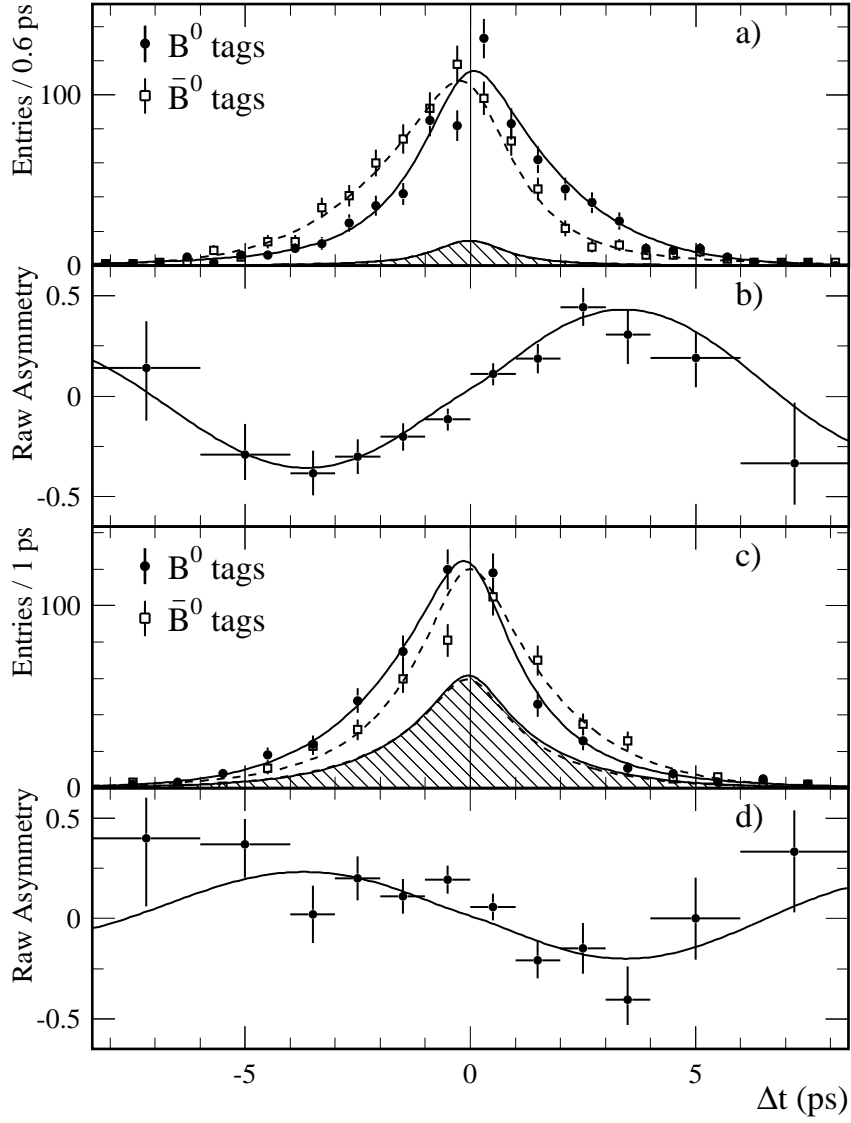
Fig. 5. a) Number of $\eta_f = -1$ candidates ($J/\psi K_S^0$, $\psi(2S)K_S^0$, $\chi_{c1}K_S^0$, and $\eta_c K_S^0$) in the signal region with a B^0 tag N_{B^0} and with a $\overline{B}^0$ tag $N_{\overline{B}^0}$, and b) the raw asymmetry $(N_{B^0} - N_{\overline{B}^0})/(N_{B^0} + N_{\overline{B}^0})$ as functions of Δt. The solid (dashed) curves represent the fit projection in Δt for B^0 ($\overline{B}^0$) tags. The shaded regions represent the background contributions. Figures c) and d) contain the corresponding information for the $\eta_f = +1$ mode $J/\psi K_L^0$.

between the suppressed $b \rightarrow u\bar{c}d$ amplitude with the favored $b \rightarrow c\bar{u}d$ amplitude for some tag-side B decays. The other sources of systematic error for $|\lambda|$ are the same as in the $\sin2\beta$ measurement.

4 CP asymmetry measurement in $B^0 \rightarrow D^{*+}D^{*-}$

Similar to the $B \rightarrow J/\psi \, K^{*0}(K_s^0\pi^0)$ final state, $B^0 \rightarrow D^{*+}D^{*-}$ is a pseudoscalar decay to a vector-vector final state, with contributions from three partial waves with different CP parities: even for the S- and D-waves, odd for the P-wave. In the model described in Ref. 19 the P-wave contribution is predicted to be about 11%. The angular distribution of the decay products can be used to measure the CP parameters of the CP-even and CP-odd components,[21] which in principle can be different due to contributions from penguin diagrams.

Up to corrections due to theoretically uncertain penguin diagram contributions,[18] the CP asymmetry in $B^0 \rightarrow D^{*+}D^{*-}$ is related to $\sin2\beta$. Penguin-induced corrections are predicted to be small in models based on the factorization approximation and heavy quark symmetry; an effect of about 2% is predicted.[20] Thus, a comparison with the $\sin2\beta$ determined in charmonium modes, as described above with that obtained in $B^0 \rightarrow D^{*+}D^{*-}$ is an important test of these models and the consistency of the Standard Model.

B^0 mesons are exclusively reconstructed by combining two charged D^* candidates reconstructed in a number of D^* and D decay modes. The D^0 and D^+ modes reconstructed are $D^0 \rightarrow K^-\pi^+$, $D^0 \rightarrow K^-\pi^+\pi^0$, $D^0 \rightarrow K^-\pi^+\pi^+\pi^-$, $D^0 \rightarrow K_s^0\pi^+\pi^-$, $D^+ \rightarrow K^-\pi^+\pi^+$, $D^+ \rightarrow K_s^0\pi^+$ and $D^+ \rightarrow K^-K^+\pi^+$. D^0 and D^+ meson candidates are required to have an invariant mass within 20 MeV/c^2 of the nominal D^0 or D^+ mass. The same interval is used for all D^0 modes except $K^-\pi^+\pi^0$, which has a looser requirement of 35 MeV/c^2 due to the momentum resolution of the π^0.

D^{*+} mesons are reconstructed in their decays $D^{*+} \rightarrow D^0\pi^+$ and $D^{*+} \rightarrow D^+\pi^0$. We include $D^{*+}D^{*-}$ combinations decaying to $(D^0\pi^+, \overline{D}^0\pi^-)$ or $(D^0\pi^+, D^-\pi^0)$, but not $(D^+\pi^0, D^-\pi^0)$ due to the smaller branching fraction and larger expected backgrounds.

If an event contains both a D^{*+} and a D^{*-} candidate, each is subjected to a mass constraint fit, and then combined to form a B candidate. The ΔE of the B^0 candidate is required to be less than 25 MeV. The resulting m_{ES} distribution is shown in Fig. 6. We find 102 tagging signal candidates with a purity of approximately 82%.

A one-dimensional angular analysis is used to determine the fraction, $R_\perp$, of the
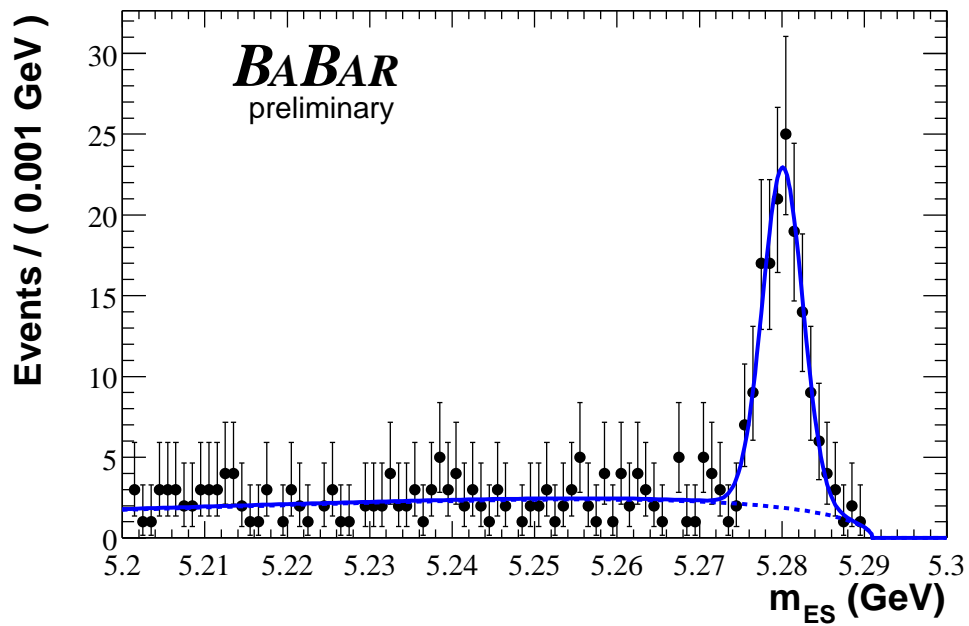
Fig. 6. The m_{ES} projection of the data for $B^0 \to D^{*+}D^{*-}$. These events are required to have $|\Delta E| < 25\,\mathrm{MeV}$. The solid (dashed) line represents the result (background component) of the fit described in the text.

CP-odd component. After acceptance correction, we find

$$R_\perp = 0.07 \pm 0.06((\text{stat})) \pm 0.03((\text{syst})), \tag{12}$$

indicating that the data is consistent with no CP-odd component in $B^0 \to D^{*+}D^{*-}$ decays. We take advantage of this in the time dependent analysis.

In principle both the magnitude and phase of λ may be different for the CP even and CP odd components in $B^0 \to D^{*+}D^{*-}$. As the statistics of the signal are limited and $R_\perp$ is small, we fix $|\lambda_\perp| = 1$ and $\mathcal{I}m\lambda_\perp = -0.741$ as expected in the Standard Model, given the $\sin2\beta$ measurement in Eq. 12. The remaining CP parameters describe the CP even contribution, which we measure to be

$$
\begin{aligned}
|\lambda_+| &= 0.98 \pm 0.25 \pm 0.09 \\
\mathcal{I}m\lambda &= 0.31 \pm 0.43 \pm 0.10, \tag{13}
\end{aligned}
$$

where the errors are statistical and systematic, respectively. This measurement is approximately 2.7σ different from the expectation if penguins were negligible ($\mathcal{I}m\,\lambda = -0.741$ and $|\lambda| = 1$). The Δt and raw asymmetry distributions for $B^0 \to D^{*+}D^{*-}$ are shown in Figure 7.

5 CP **asymmetry measurement in** $B^0 \to J/\psi\pi^0$

The decay $B^0 \to J/\psi\,\pi^0$ is a Cabibbo-suppressed $b \to c\bar{c}d$ decay, whose tree contribution has the same weak phase as the $b \to c\bar{c}s$ modes (e.g. $B^0 \to J/\psi\,K_S^0$). A portion of the penguin contribution has a different weak phase, which may give a time-dependent CP asymmetry that differs from the one observed in $b \to c\bar{c}s$ decays. As the tree contribution is Cabibbo suppressed, the penguin diagrams may give a similar contribution to the decay rate. The absence of penguin contributions would give $S_{J/\psi\,\pi^0} = -\sin2\beta$ and $C_{J/\psi\,\pi^0} = 0$.

$B^0 \to J/\psi\,\pi^0$ candidates are selected by identifying $J/\psi \to e^+e^-$ or $J/\psi \to \mu^+\mu^-$ decays and $\pi^0 \to \gamma\gamma$ decays (details are given elsewhere[22]). Several kinematic and topological variables are linearly combined using a Fisher discriminant, $\mathcal{F}$, to provide additional separation between signal and $e^+e^- \to u\bar{u}, d\bar{d}, s\bar{s}, c\bar{c}$ (continuum) background events. The remaining sources of background are $B \to J/\psi\,K_S^0(\pi^0\pi^0)$, other $B \to J/\psi\,X$ decays, and random combinatorics from $B\bar{B}$ and $q\bar{q}$ decays. Figure 8 shows the m_{ES} distribution after a cut on ΔE. The signal region contains 49 events with approximately a 59% purity.
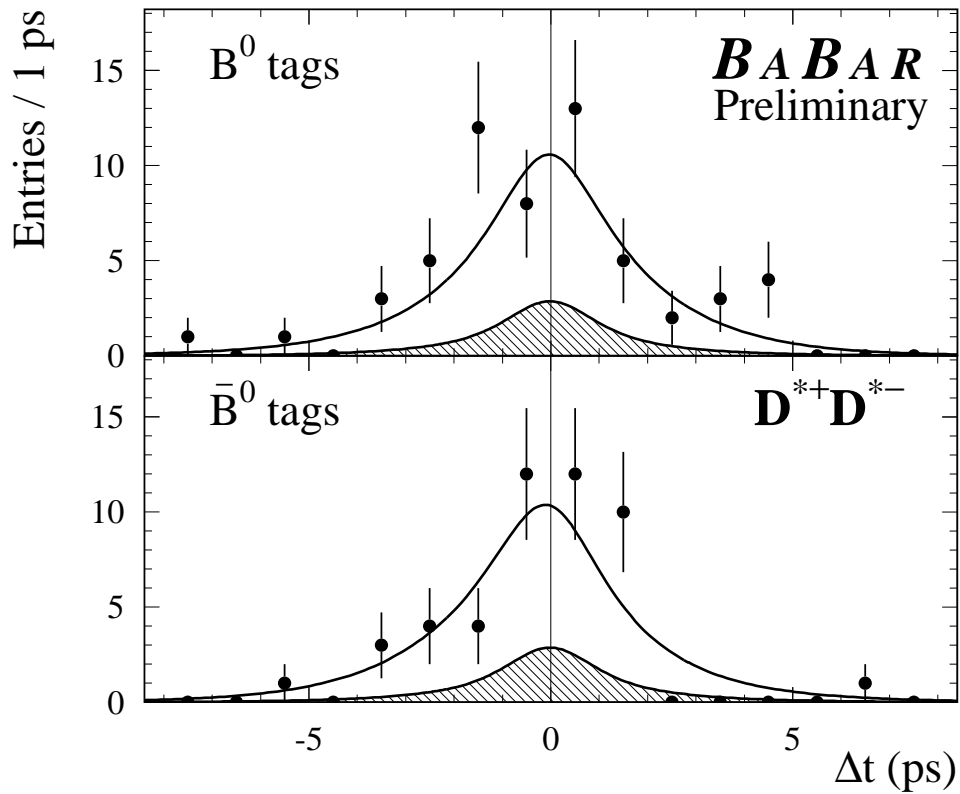
Fig. 7. The Δt projections of the data for $B^0 \to D^{*+}D^{*-}$. These events are required to have $|\Delta E| < 25\,\mathrm{MeV}$ and $m_{\mathrm{ES}} > 5.27\,\mathrm{MeV}/c^2$. The hatched region shows the background expectation.
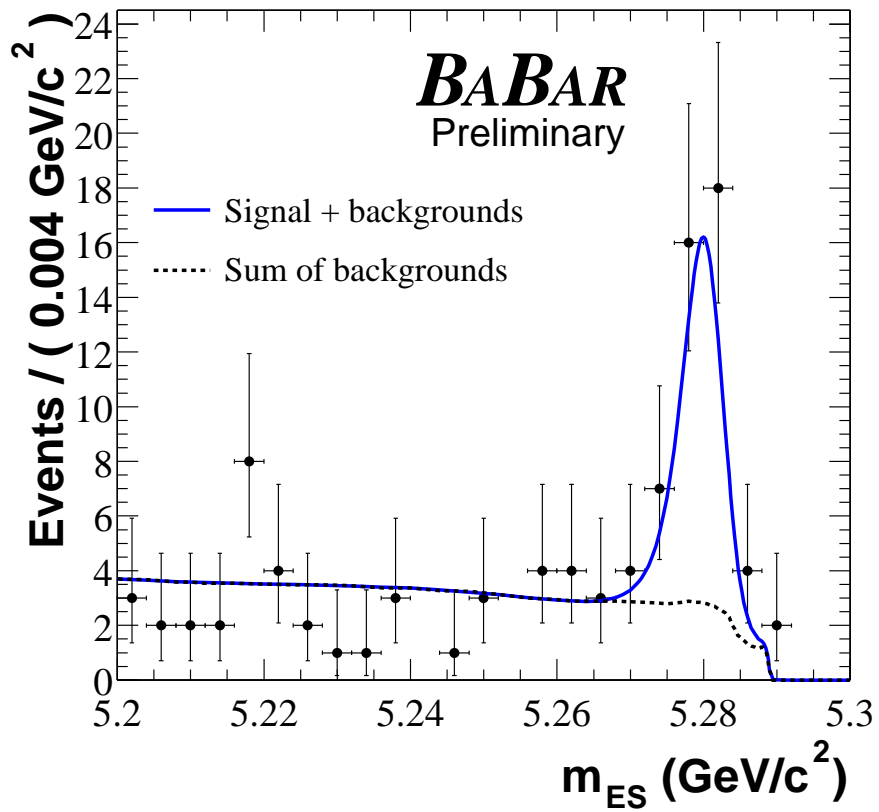
Fig. 8. Distribution of m_{ES} for $B \to J/\psi\,\pi^0$ candidate events with $\Delta E < 0.11$ GeV. The dashed line shows the expected background contribution.

The CP violating parameters are measured using an unbinned maximum likelihood fit including the Δt, m_{ES}, and ΔE variables to fully discriminate signal from the backgrounds. The probability density functions are taken from data whenever possible, otherwise from Monte Carlo simulations. Two-dimensional PDFs are used for the m_{ES} and ΔE distributions, as they are correlated for the $B \rightarrow J/\psi\, X$ and $B \rightarrow J/\psi\, K_S^0$ backgrounds. The Δt distribution of $B \rightarrow J/\psi\, K_S^0(\pi^0\pi^0)$ assumes the $\sin 2\beta$ measured above by the $b \rightarrow c\bar{c}s$ charmonium-containing channels.

We measure

$$
\begin{aligned}
C_{J/\psi\,\pi^0} &= 0.38 \pm 0.41(\mathrm{stat}) \pm 0.09(\mathrm{syst}), \\
S_{J/\psi\,\pi^0} &= 0.05 \pm 0.49(\mathrm{stat}) \pm 0.16(\mathrm{syst}),
\end{aligned}
\tag{14}
$$

where the systematic errors dominated by the determination of the PDF parameters.

6 CP asymmetry measurement in $B^0 \rightarrow \phi K_S^0$

The charmless B meson decays into final states with a ϕ meson are interesting because they are dominated by $b \rightarrow s(d)s\bar{s}$ gluonic penguins, with a smaller contribution from electroweak penguins, while other Standard Model contributions are highly suppressed. These decays allow the clean extraction of the CP-violating parameter $\sin 2\beta$. Comparison of the value of $\sin 2\beta$ obtained from these modes with that from charmonium modes probes for new physics participating in penguin loops.[23,24] The predicted deviation of $\sin 2\beta$ for the ϕK^0 mode in the Standard Model is smaller than 4%.[25] The decay of neutral B mesons to the $\eta_f = -1$ final state ϕK^0 has been observed by *BABAR* in a sample of about 45 million B mesons with a branching fraction of $BF(B^0 \rightarrow \phi K^0) = (8.1^{+3.1}_{-2.5} \pm 0.8) \times 10^{-6}$.[26]

We fully reconstruct B meson candidates (B_{CP}) in the decay mode ϕK_S^0 with $K_S^0 \rightarrow \pi^+\pi^-$ and $\phi \rightarrow K^+K^-$,

Monte Carlo simulation demonstrates that contamination from other B decays is negligible. However, charmless hadronic modes suffer from backgrounds due to random combinations of tracks produced in $\bar{q}q$ continuum events. The distinguishing feature of such backgrounds is their characteristic event shape resulting from the two-jet production mechanism.

As with the $B^0 \rightarrow J/\psi\, \pi^0$ analysis, an unbinned maximum likelihood fit is performed using Δt, as well as variables that distinguish signal from the continuum backgrounds.
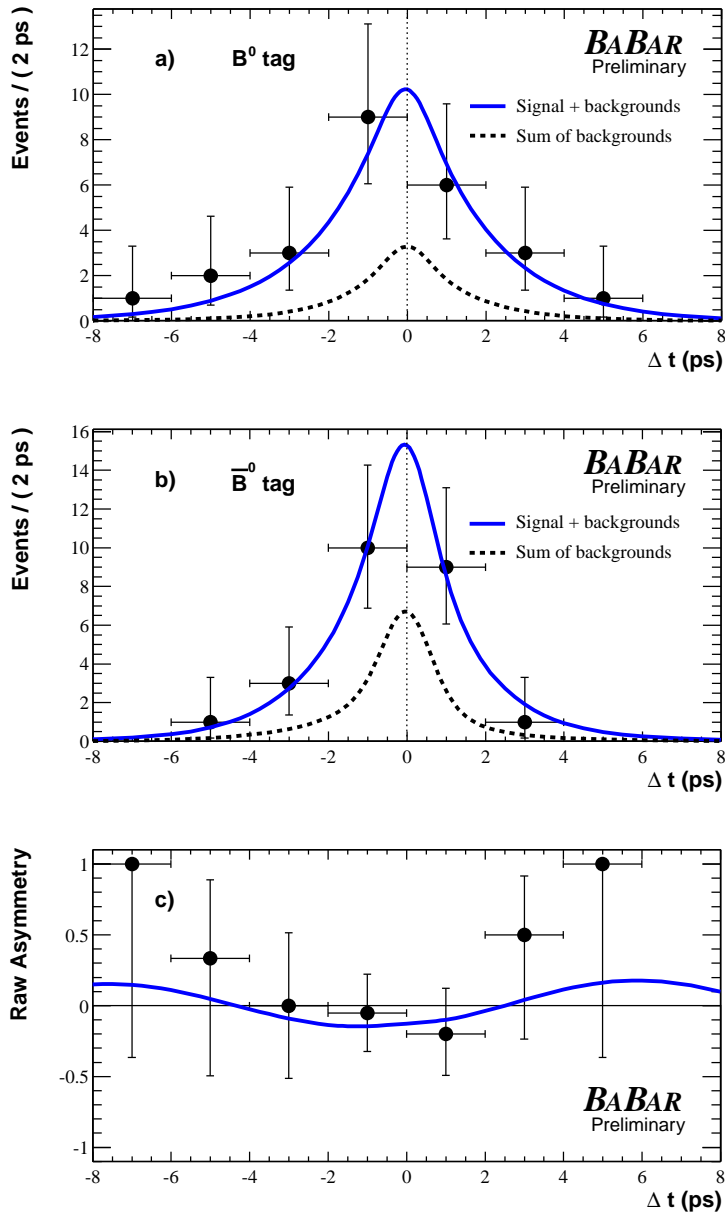
Fig. 9. Number of $B \rightarrow J/\psi\,\pi^0$ candidates in the signal region a) with a B^0 tag N_{B^0} and b) with a $\overline{B}^0$ tag $N_{\overline{B}^0}$, and c) the raw asymmetry $(N_{B^0} - N_{\overline{B}^0})/(N_{B^0} + N_{\overline{B}^0})$, as functions of Δt. Candidates in these plots are required to satisfy $-0.11 < \Delta E < 0.11\,\mathrm{GeV}$ and $m_{\mathrm{ES}} > 5.27\,\mathrm{GeV}/c^2$. The curves in a) and b) are projections that use the values of the other variables in the likelihood to determine the contribution to the signal or one of the backgrounds.
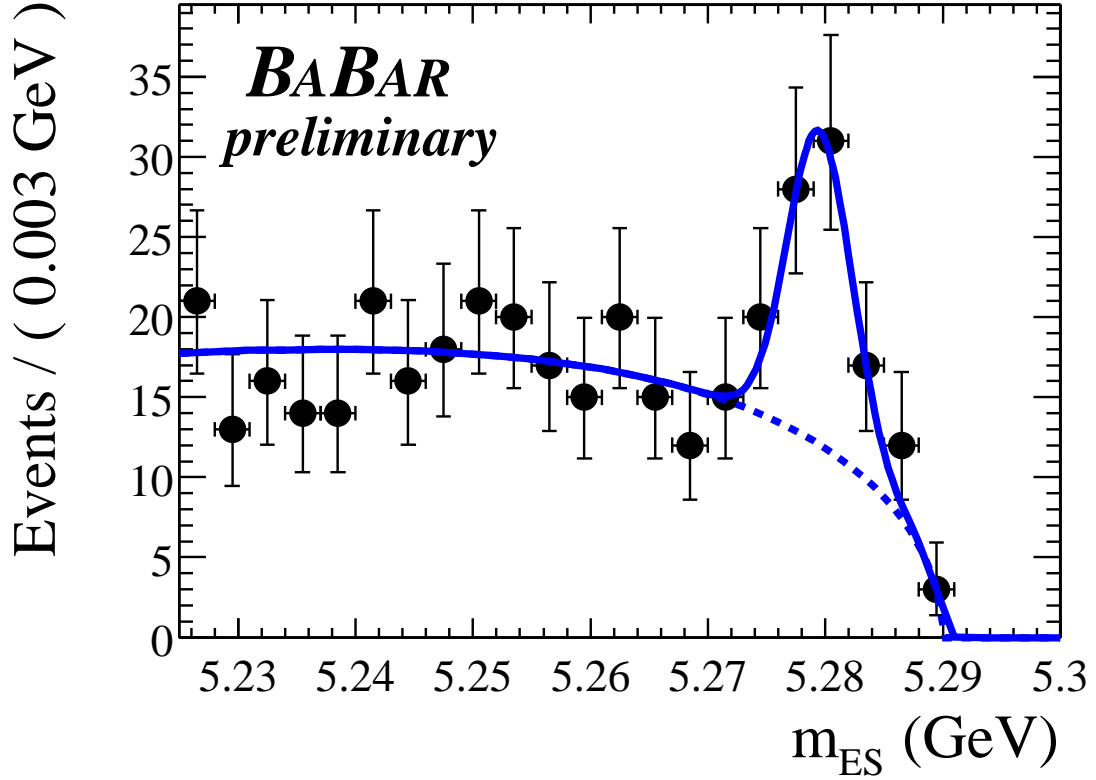
Fig. 10. Distribution of m_{ES} for ϕK_s^0 candidates. The solid line refers to the fit for all events, the dashed line corresponds to the expected background distribution.

These include m_{ES}, ΔE, and a Fisher discriminant ($\mathcal{F}$). Figure 10 shows the m_{ES} distribution enhanced in signal using a cut on the likelihood for each event. In this region, we observe 66 signal candidates with a purity of approximately 50%.

We measure

$$\sin 2\beta = -0.19^{+0.52}_{-0.50}(\text{stat}) \pm 0.09(\text{syst}), \tag{15}$$

where the errors are statistical and systematic.

7 CP asymmetry measurement in $B^0 \to \pi^+\pi^-$

The time-dependent CP-violating asymmetry in the decay $B^0 \to \pi^+\pi^-$ is related to the angle α, and ratios of branching fractions for various $\pi\pi$ and $K\pi$ decay modes are sensitive to the angle γ. Here we present results for the CP-violating asymmetries in $B^0 \to \pi^+\pi^-$. More details on the analysis technique are given elsewhere.[27]

We reconstruct a sample of neutral B mesons (B_{rec}) decaying to the $h^+h'^-$ final state,
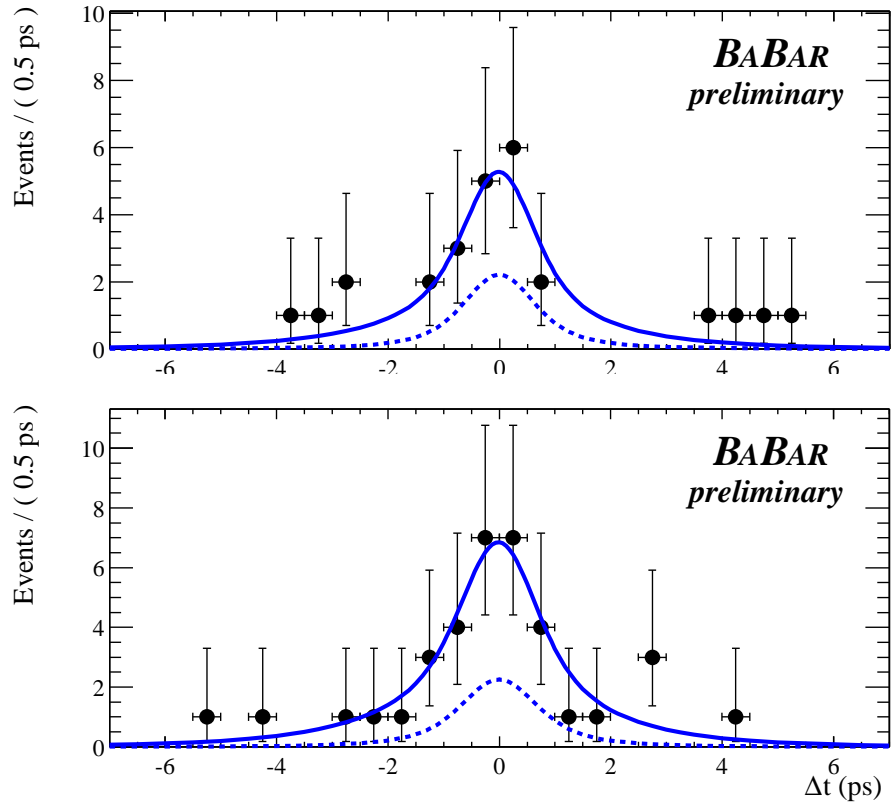
Fig. 11. Time distributions for signal region $B \to \phi K_s^0$ candidates with B^0 (top) and $\bar{B}^0$ (bottom) tags. The solid line refers to the fit for all events, the dashed line corresponds to background.

where h and h' refer to π or K. Signal yields are determined with a maximum likelihood fit including kinematic, topological, and particle identification information. The fitted signal yields are $157 \pm 19 \pm 7$ for $B^0 \to \pi^+\pi^-$ and $589 \pm 30 \pm 17$ for $B^0 \to K^+\pi^-$. In addition we determine $A_{K^+\pi^-} = -0.102 \pm 0.050 \pm 0.016$.

The parameters $S_{\pi\pi}$ and $C_{\pi\pi}$ are determined from a second fit including tagging and Δt information, where the B_{flav} sample is included to determine the signal parameters describing tagging information and the Δt resolution function. A total of 76 parameters are varied in the fit, including the values of $S_{\pi\pi}$ and $C_{\pi\pi}$ (2); signal and background yields (5); $K\pi$ charge asymmetries (2); signal and background tagging efficiencies (16) and efficiency asymmetries (16); signal mistag fraction and mistag fraction differences (8); signal resolution function (9); and parameters for the background shapes in m_{ES} (5), ΔE (2), $\mathcal{F}$ (5), and Δt (6). We assume zero events from $B^0 \to K^+K^-$ decays and we fix τ_{B^0} and Δm_d to their world average values.[17] As a means of validating the analysis technique, we determine τ and Δm_d in the B_{rec} sample and find $\tau = (1.56 \pm 0.07)\,\text{ps}$ and $\Delta m_d = (0.52 \pm 0.05)\,\text{ps}^{-1}$.

The combined fit to the B_{rec} and B_{flav} samples yields

$$
\begin{aligned}
S_{\pi\pi} &= 0.02 \pm 0.34\,(\text{stat}) \pm 0.05\,(\text{syst})\ [-0.54, +0.58], \\
C_{\pi\pi} &= -0.30 \pm 0.25\,(\text{stat}) \pm 0.04\,(\text{syst})\ [-0.72, +0.12],
\end{aligned}
$$

where the range in square brackets indicates the 90% C.L. interval taking into account the systematic errors. The correlation between $S_{\pi\pi}$ and $C_{\pi\pi}$ is -10%.

Systematic uncertainties on $S_{\pi\pi}$ and $C_{\pi\pi}$ are dominated by imperfect knowledge of the PDF shapes and possible fit bias. Using the *BABAR* upper limit on $\mathcal{B}(B^0 \to \pi^0\pi^0)$ and the isospin relations for $B \to \pi\pi$[28] we find

$$
|\alpha_{\text{eff}} - \alpha| < 51° \tag{16}
$$

at 90% confidence level.

8 CP **asymmetry measurement in** $B^0 \to \rho\pi$ **and** $B^0 \to \rho K$

We investigate CP violation using charmless $B^0/\overline{B}^0$ decays to $\pi^+\pi^-\pi^0$ and $K^\mp\pi^\pm\pi^0$ dominated by the $\rho^\pm h^\mp$ intermediate state, where $h = \pi$ or K. As in the case of $\pi^+\pi^-$, the $\rho\pi$ mode provides a probe of both direct CP violation and CP violation in
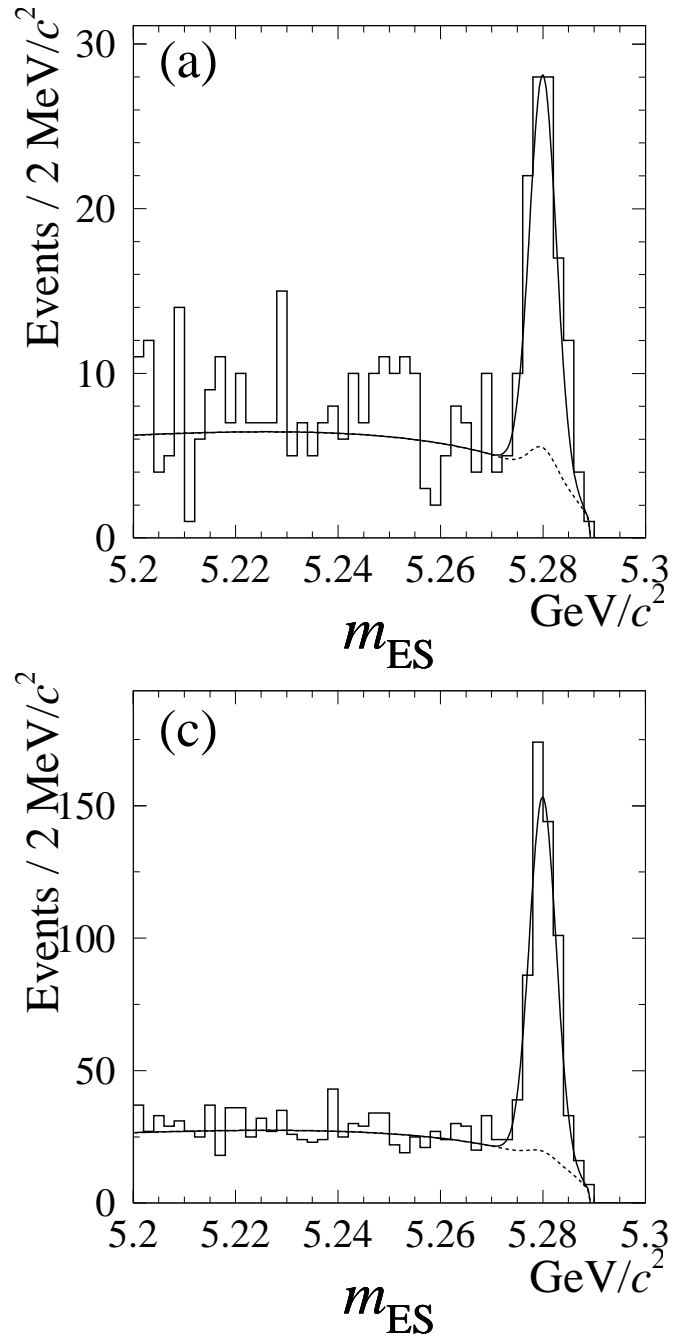
Fig. 12. Distributions of m_{ES} for events enhanced in signal (top) $\pi^+\pi^-$ and (bottom) $K^{\mp}\pi^{\pm}$ decays. Solid curves represent projections of the maximum likelihood fit, dashed curves represent $q\bar{q}$ and $\pi\pi \leftrightarrow K\pi$ cross-feed background.
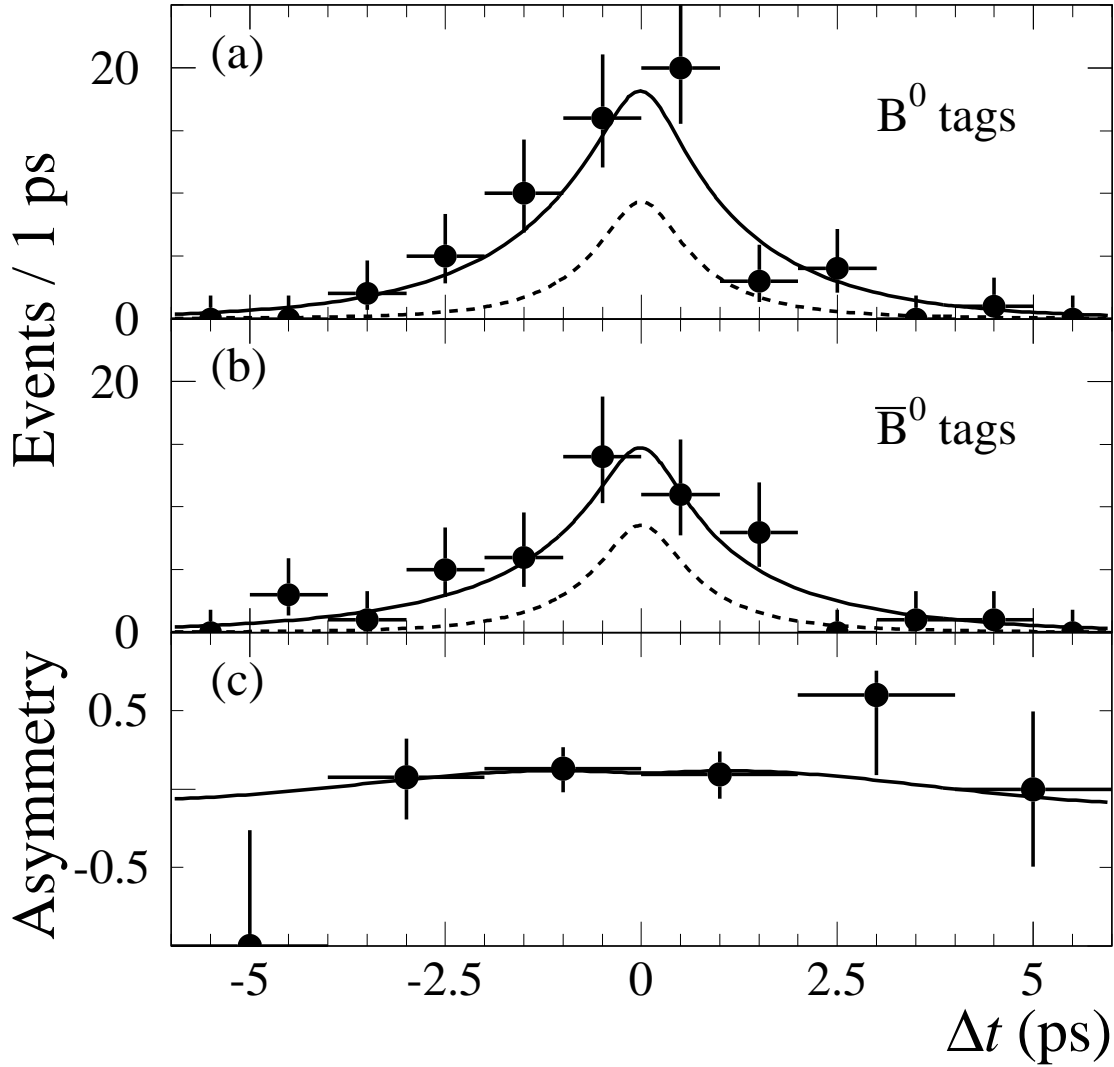
Fig. 13. Distributions of Δt for events enhanced in signal $\pi\pi$ decays with B_{tag} tagged as (a) B^0 (N_{B^0}) or (b) $\overline{B}^0$ ($N_{\overline{B}^0}$), and (c) the asymmetry $[N_{B^0} - N_{\overline{B}^0}]/[N_{B^0} + N_{\overline{B}^0}]$ as a function of Δt. Solid curves represent projections of the maximum likelihood fit, dashed curves represent the sum of $q\bar{q}$ and $K\pi$ background events.

the interference between mixing and decay amplitudes. The latter type of CP violation is related to the angle α. In contrast to $\pi^+\pi^-$, $\rho^\pm\pi^\mp$ is not a CP eigenstate and four configurations $(B^0(\overline{B}^0) \to \rho^\pm\pi^\mp)$ have to be considered. Although this leads to a more complex analysis,[29] it benefits from a higher branching fraction $(20 - 30 \times 10^{-6})$.[30,31]

The ρ resonance is broad $(150~\text{MeV}/c^2)$ and the $\rho^\pm\pi^\mp$ state may receive contributions at the amplitude level from other decay channels (*e.g.*, $B^0 \to \rho'^+\pi^-$). For this analysis, we restrict ourselves to the two regions of the $h^\pm\pi^\mp\pi^0$ Dalitz plot dominated by ρh and assign a label, ρ^+h^- or ρ^-h^+, to each event depending on the kinematics of the $h^\pm\pi^\mp\pi^0$ final state. In the following, we will use the ρ^+h^- or ρ^-h^+ labels with the above meaning.

The decay rate distributions can be written as[32]

$$
\begin{aligned}
f^{\rho^\pm h^\mp}_{B^0\text{tag}}(\Delta t) = (1 \pm A^{\rho h}_{CP})\frac{e^{-|\Delta t|/\tau}}{4\tau}\Big[1 \;\; &+\;\; \Big((S_{\rho h} \pm \Delta S_{\rho h})\sin(\Delta m_d \Delta t) \\
&-\;\; (C_{\rho h} \pm \Delta C_{\rho h})\cos(\Delta m_d \Delta t)\Big)\Big], \\
f^{\rho^\pm h^\mp}_{\overline{B}^0\text{tag}}(\Delta t) = (1 \pm A^{\rho h}_{CP})\frac{e^{-|\Delta t|/\tau}}{4\tau}\Big[1 \;\; &-\;\; \Big((S_{\rho h} \pm \Delta S_{\rho h})\sin(\Delta m_d \Delta t) \\
&-\;\; (C_{\rho h} \pm \Delta C_{\rho h})\cos(\Delta m_d \Delta t)\Big)\Big],
\end{aligned}
\tag{17}
$$

where ΔS and ΔC are insensitive to CP violation.

An unbinned maximum likelihood fit is used to distinguish $B \to \rho h$ signal events from background as well as $\rho\pi$ events from ρK events. In addition to Δt, the variables m_{ES}, ΔE and the output of a neural network algorithm discriminate signal from background, while the Cherenkov angle and, to a lesser extent, ΔE constrain the relative amount of $B \to \rho\pi$ and $B \to \rho K$.

We measure

$$
\begin{aligned}
A^{\rho K}_{CP} &= 0.19 \pm 0.14~\text{(stat)} \pm 0.11~\text{(syst)}, \\
A^{\rho\pi}_{CP} &= -0.22 \pm 0.08~\text{(stat)} \pm 0.07~\text{(syst)}, \\
C_{\rho\pi} &= 0.45~^{+0.18}_{-0.19}~\text{(stat)} \pm 0.09~\text{(syst)}, \\
S_{\rho\pi} &= 0.16 \pm 0.25~\text{(stat)} \pm 0.07~\text{(syst)}. \\
\Delta C_{\rho\pi} &= 0.38~^{+0.19}_{-0.20}~\text{(stat)} \pm 0.11~\text{(syst)}, \\
\Delta S_{\rho\pi} &= 0.15 \pm 0.26~\text{(stat)} \pm 0.05~\text{(syst)}.
\end{aligned}
\tag{18}
$$
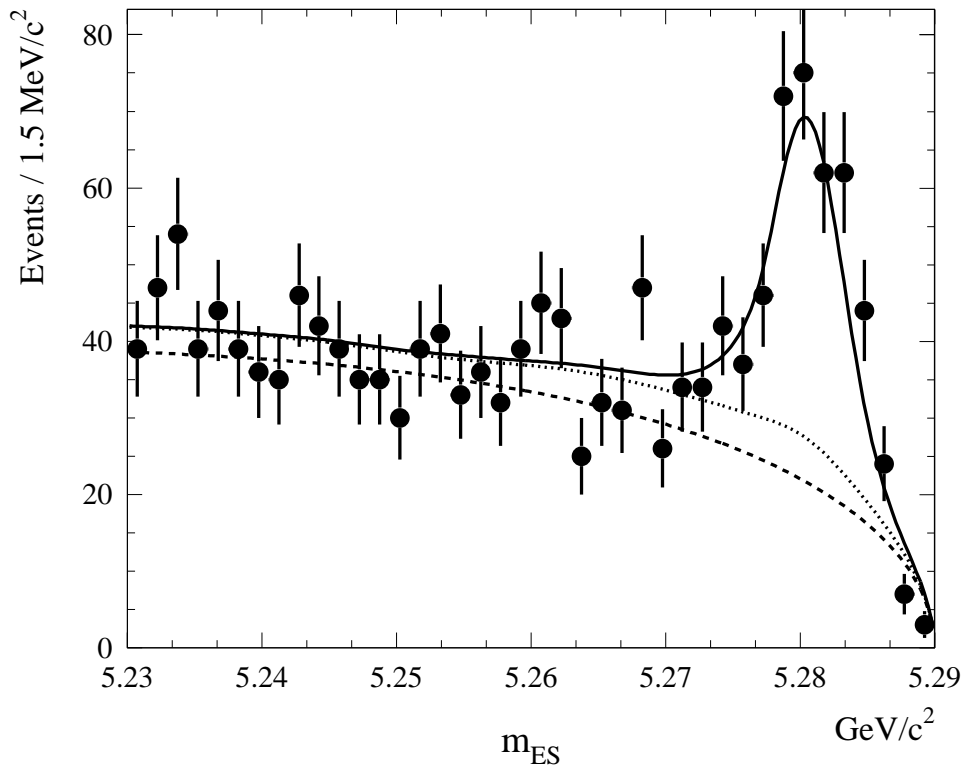
Fig. 14. Distribution of m_{ES} for samples enhanced in $\rho\pi$ signal using cuts on likelihood ratios. The solid curve represents a projection of the maximum likelihood fit result. The dashed curve represents the contribution from continuum events ($\rho\pi$ and ρK candidates combined), and the dotted line indicates the combined contributions from continuum events and B-related backgrounds, including ρK.

where the errors are statistical and systematic, respectively. The dominant source of systematic error is backgrounds from B decays. We use a Monte Carlo simulation to estimate this background source including either measured branching fractions or upper limits where available, or estimates based on related measured decay modes. A large source of B related backgrounds are from other charmless decay modes such as $B \to \rho\rho$ and $B^{\pm} \to \rho^0\pi^{\pm}$.
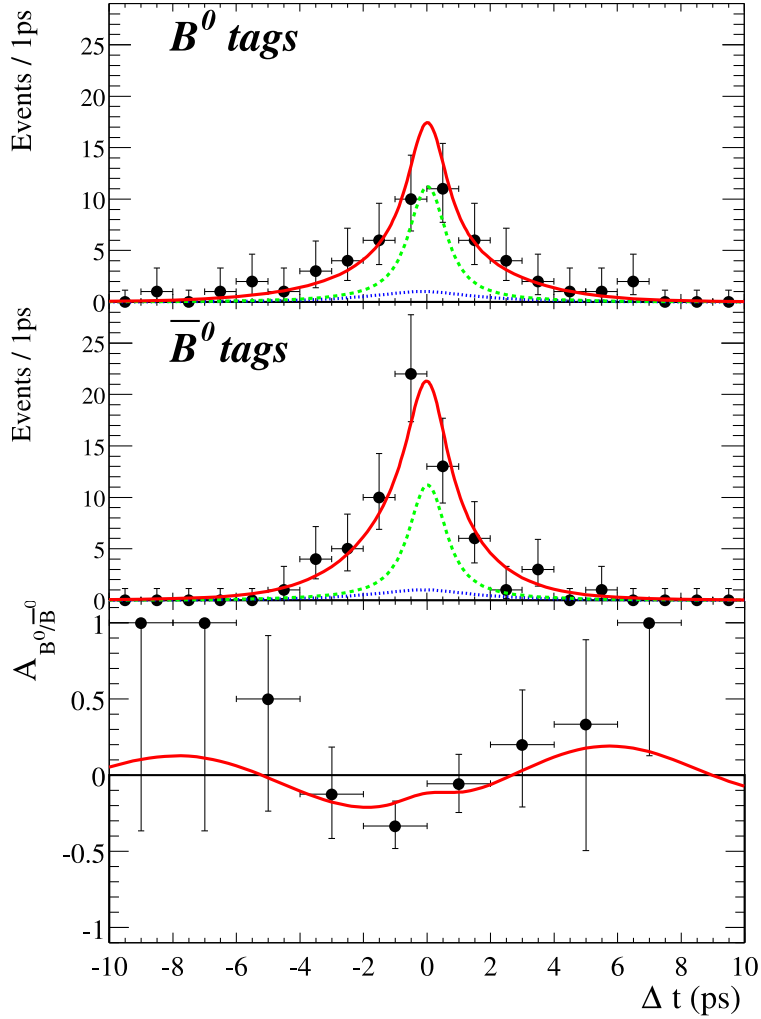
Fig. 15. Time distribution and asymmetry for B^0_{tag} and $\overline{B}^0_{\mathrm{tag}}$ decaying to $\rho\pi$, in the Lepton and Kaon categories. The sample was enriched in signal events by applying a cut on the signal-to-continuum likelihood ratio. The solid curve is a likelihood projection of the result of the full fit, and is normalized to the expected number of events according to that fit (71 signal events, 36 continuum background events and 10 B background events). The dotted line is the contribution from B-related backgrounds and the dashed line is the total B and continuum background contribution. The depression around zero in the asymmetry plot is due to the relatively large fraction of continuum events in this region of Δt. The non-zero central value for the CP parameter $\S_{\rho\pi}$ induces a small contribution to the asymmetry that is odd in Δt.

9   Conclusion

We have presented results on a number of time-dependent CP asymmetries in neutral B decays using a data sample of approximately 88 million $B\bar{B}$ pairs collected by the *BABAR* detector. Our measurement of $\sin2\beta$ using $B^0 \rightarrow (c\bar{c})K^0_S$ and $B^0 \rightarrow J/\psi K^0_L$ decays agrees well with the Standard Model expectation. Other measurements are currently statistics limited, but with higher statistics will soon provide important tests of the consistency of the CKM picture.

10   Acknowledgments
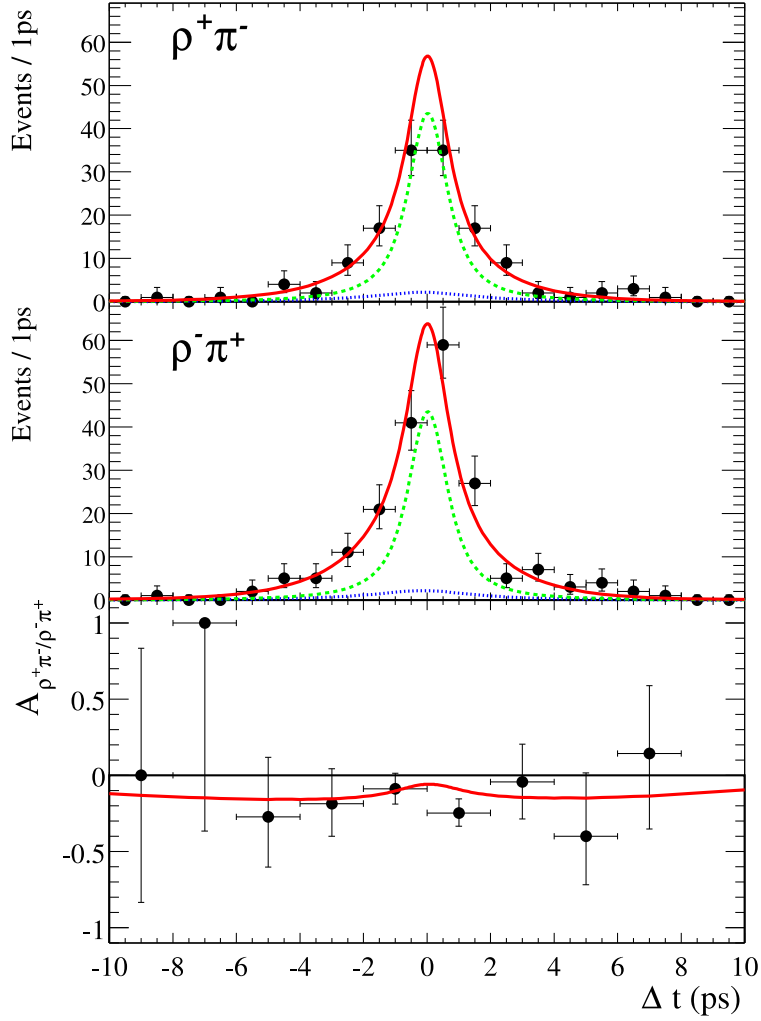
Fig. 16. Time distribution and asymmetry $A_{\rho^+\pi^-/\rho^-\pi^+}$ between $\rho^+\pi^-$ and $\rho^-\pi^+$ for all the tagging categories. The sample was enriched in signal events by applying a cut on the signal-to-continuum likelihood ratio. The solid curve is a likelihood projection of the result of the full fit, and is normalized to the expected number of events according to that fit (156 signal events, 157 continuum background events and 21 B background events). The dotted line is the contribution from B-related backgrounds and the dashed line is the total B and continuum background contribution. The depression around zero in the asymmetry plot is due to continuum dilution. In the absence of continuum background, the asymmetry curve would be flat and equal to $A_{CP}^{\rho\pi}$ defined in Eq. 17.

References

[1] B. Aubert *et al.* (*BABAR* Collaboration) Phys. Rev. Lett. **89**, 201802, (2002).

[2] B. Aubert *et al.* (*BABAR* Collaboration), hep-ex/0207055. Submitted to Phys. Rev. Lett. (2002).

[3] B. Aubert *et al.* (*BABAR* Collaboration), hep-ex/0207058. Submitted to 31st International Conference on High Energy Physics (Amsterdam, 2002).

[4] B. Aubert *et al.* (*BABAR* Collaboration), hep-ex/0207068. Submitted to 31st International Conference on High Energy Physics (Amsterdam, 2002).

[5] B. Aubert *et al.* (*BABAR* Collaboration), hep-ex/0207070. Submitted to 31st International Conference on High Energy Physics (Amsterdam, 2002).

[6] B. Aubert *et al.* (*BABAR* Collaboration), hep-ex/0207072. Submitted to 31st International Conference on High Energy Physics (Amsterdam, 2002).

[7] B. Aubert *et al.* (*BABAR* Collaboration), *Nucl. Instr. and Methods* **A479**, 1 (2002).

[8] N. Cabibbo, Phys. Rev. Lett. **10** 531 (1963). M. Kobayashi and T. Maskawa, *Prog. Theor. Phys.* **49**, 652 (1973).

[9] See, for example, F. J. Gilman, K. Kleinknecht, and B. Renk, *Phys. Rev* **D15**, 010001 (2002).

[10] See, for example, L. Wolfenstein, Phys. Rev. **D66**, 010001 (2002).

[11] B. Aubert *et al.* (*BABAR* Collaboration), Phys. Rev. Lett. **87**, 241801 (2001).

[12] B. Aubert *et al.* (*BABAR* Collaboration), Phys. Rev. Lett. **87**, 091801 (2001).

[13] K. Abe *et al.* (BELLE Collaboration), Phys. Rev. Lett. **87**, 091802 (2001).

[14] *BABAR* Collaboration, B. Aubert *et al.*, SLAC-PUB-9060, hep-ex/0201020, to appear in Phys. Rev.D.

[15] Charge conjugation is implied throughout this note, unless explicitly stated.

[16] ARGUS Collaboration, H. Albrecht *et al.*, 543 (1990).

[17] Particle Data Group, K. Hagiwara *et al.*, Phys Rev **D66**, 010001 (2002).

[18] A.I. Sanda and Z.Z. Xing, Phys. Rev. D **56**, 341 (1997).

[19] Z.Z. Xing, Phys. Rev.Phys. Rev. D **61**, 014010 (2000).

[20] X.Y. Pham and Z.Z. Xing, Phys. Rev. B **458**, 375 (1999).

[21] I. Dunietz, *et al.*, Phys. Rev. D **43**, 2193 (1991).

[22] B. Aubert *et al.* (*BABAR* Collaboration), Phys. Rev. D **65**, 032001 (2002).

[23] Y. Grossman and M.P. Worah, Phys. Lett. B **395**, 241 (1997).

[24] R. Fleischer, Int. J. Mod.Phys. A**12**, 2459 (1997).

[25] Y. Grossman, G. Isidori, and M.P. Worah, Phys. Rev. D **58**, 057505 (1998).

[26] B. Aubert *et al.* (*BABAR* Collaboration), Phys. Rev. Lett. **87**, 151801-1 (2001).

[27] B. Aubert *et al.* (*BABAR* Collaboration), Phys. Rev. Lett. **87**, 151802 (2001); Phys. Rev. D **65**, 051502 (2002).

[28] Y. Grossman and H. R. Quinn, Phys. Rev. D **58**, 017504 (1998).

[29] R. Aleksan, I. Dunietz, B. Kayser and F. Le Diberder, Nuclear Physics **B361**, 141 (1991).

[30] B. Aubert *et al.* (*BABAR* Collaboration), hep-ex/0107058, contribution to the 20th International Symposium on Lepton and Photon Interactions at High Energies, Rome, Italy (2001).

[31] A. Gordon *et al.* (Belle Collaboration), hep-ex/0207007, submitted to Phys. Lett. **B**.

[32] The *BABAR* Physics Book, Editors P.F. Harrison and H.R. Quinn, SLAC-R-504 (1998).